Nickel-Induced Oligomerization of the Histidine-Rich Metallochaperone CooJ from Rhodospirillum Rubrum

Marila Alfano, Julien Pérard, Christine Cavazza

inorganics

MDPI

Communication

Nickel-Induced Oligomerization of the Histidine-Rich Metallochaperone CooJ from *Rhodospirillum Rubrum*

Marila Alfano, Julien Pérard and Christine Cavazza *

Univ. Grenoble Alpes, CEA, CNRS, CBM, F-38000 Grenoble, France
* Correspondence: christine.cavazza@cea.fr

Received: 27 May 2019; Accepted: 25 June 2019; Published: 1 July 2019

Abstract: [NiFe]-carbon monoxide dehydrogenase reversibly catalyzes the oxidation of CO to CO_2. Its active site is a unique $NiFe_4S_4$ cluster, known as C-cluster. In *Rhodospirillum rubrum*, three nickel-dependent proteins, CooC, CooT and CooJ are required for Ni insertion into the active site. Among them, CooJ is a histidine-rich protein, containing two distinct and spatially separated Ni(II)-binding sites: a strictly conserved N-terminal site and a variable histidine tail at the C-terminus. Here, using biophysical techniques, we study the behavior of the protein upon Ni(II) addition. Using circular dichroism and chemical denaturation, we show that the binding of Ni(II) to the protein increases its stability. Moreover, high-order oligomers are formed through nickel–histidine tail interactions, both in vitro and in cellulo, via a dynamical and reversible process.

Keywords: histidine-rich protein; carbon monoxide dehydrogenase; nickel chaperone; nickel-induced oligomerization

1. Introduction

Monofunctional nickel-dependent carbon monoxide dehydrogenases (CODH) reversibly catalyzes the oxidation of CO to CO_2 [1]. CODH's active site, called C-cluster, is a $NiFe_4S_4$ cluster, unique in biology, whose atypical nature was revealed by X-ray crystallography [2,3]. In the hydrogenogenic carboxydotroph *Rhodospirillum rubrum*, CODH plays an essential role in the energy metabolism when CO is the sole energy source [4]. In this bacterium, the structural gene of CODH, called *cooS*, is found in the *cooFSCTJ* operon [5]. Three of the proteins encoded by the *coo* operon, namely CooC, CooT and CooJ, are nickel chaperones dedicated to nickel insertion into CODH, while CooF is a ferredoxin [6]. In vivo studies have shown that the ATPase CooC and the Ni(II)-binding proteins CooT and CooJ play a significant role in the maturation pathway leading to a fully active enzyme. Moreover, Ni insertion is a key step in the enzyme activation process [5,7]. Among these chaperones, CooJ from *R. rubrum* (*Rr*CooJ) is a histidine-rich protein, with a histidine tail comprising 16 histidines and 2 cysteines at its C-terminus [8]. Initially thought to be only present in *R. rubrum*, our recent study revealed the existence of at least 46 CooJ homologues in bacteria [9]. In solution, *Rr*CooJ forms a 25-kDa homodimer with a central coiled coil and two independent C-terminal his-tails and possesses several Ni(II) binding sites. The first one is present in the N-terminal region and binds one Ni(II) per dimer via a "H-X3-H-X3-H" motif, strictly conserved in the CooJ family. In addition, the two Histidine-rich regions bind at least 2 Ni(II) ions each (Figure 1), via both histidine and cysteine residues, as shown by site-directed mutagenesis of cysteines 109 and 111 that led to decreased stoichiometry [9].

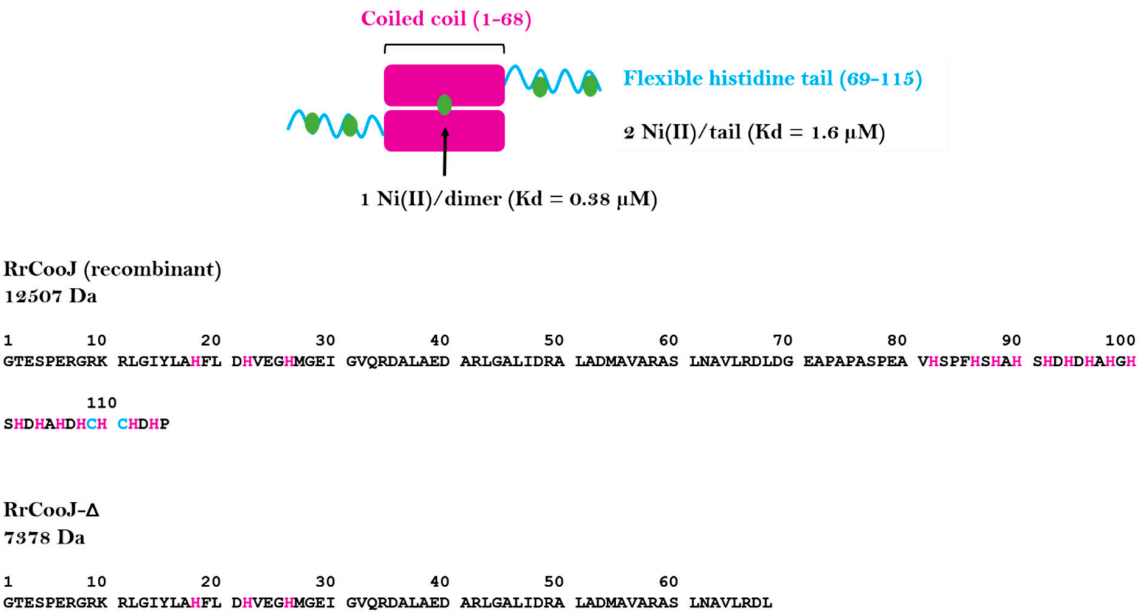

Figure 1. Schematic representation of *Rr*CooJ and its amino acid sequence. Ni(II) ions are depicted as green spheres. Histidine residues are depicted in magenta and cysteines 109 and 111 are in blue.

Histidine-rich proteins, such as histatin 5 or aß peptides [10], are predicted to be intrinsically disordered with a tendency to form oligomers driven either by self-association or through interaction with multivalent ions. In nickel chaperones, the presence of histidine-rich regions is often proposed to be related to nickel storage, and/or detoxification, due to their ability to quickly bind and release nickel ions. Among them, one remarkable example is Hpn from *Helicobacter pylori*, a small protein of 7 kDa composed of histidines for about half of the total amino-acid sequence, which is expected to form high-order oligomers, with 20-mers as predominant species, even in the absence of metal [11].

Here, we report the behavior of *Rr*CooJ towards nickel in vitro and in cellulo, using a combination of biophysical techniques. *Rr*CooJ exists as an equilibrium of oligomeric states in solution in the presence of Ni(II) ions, while the apo-protein forms a stable dimer. We reveal that the His-rich region is responsible for the oligomeric process.

2. Results

Recently, we showed that the two histidine tails present in *Rr*CooJ are highly flexible and predicted to be partly disordered [9]. Moreover, Ni addition to the apo-dimer led to its conformational change, as observed by size-exclusion chromatography coupled to multi-angle laser light scattering (SEC-MALLS) experiments. Here we used circular dichroism (CD) in the far UV region (190–250 nm) and chemical denaturation of *Rr*CooJ, either in its apo- or holo-form (Ni-*Rr*CooJ), to get more information about the impact of Ni(II) ions on *Rr*CooJ conformation. The CD spectrum of apo-*Rr*CooJ is characterized by a positive peak at 193 nm and two negative peaks at 220 nm and 208 nm, attributed to the presence of a high α-helix content in its secondary structures. Upon the addition of Ni(II) ions to the apo-protein solution, the negative peaks increased gradually, as an index of a conformational change (Figure 2a). Quantitative analysis, performed using the web server BeStSel [12], showed that the increase in ellipticity was correlated to a slight increase in the helical content (from 83% for apo-*Rr*CooJ to 85% for Ni-*Rr*CooJ) and a decrease in the turns content (from 6% for apo-*Rr*CooJ to 0.4% for Ni-*Rr*CooJ). Interestingly, the CD signal at 208 nm saturated when the Ni(II) concentration reached 20 µM, corresponding to 5 molar eq. of Ni(II) per dimer, the same stoichiometry as the one previously determined by ITC (Figure 2b). Considering the predominance of α-helices in the protein, the $\Theta_{222/208}$ ratio, which increases if the protein gains in stability [13], can be used to get information about *Rr*CooJ's behavior towards nickel. For a Ni(II) concentration greater than 12 µM

(corresponding to 3 molar eq. of Ni(II)), the ratio is >1, reflecting an increase in the α-helix content and likely the stabilization of the protein. To further investigate the difference in stability between the apo- and the holo-forms, chemical denaturation using guanidine hydrochloride (GuCl) was performed. Their stability was compared by monitoring the variation of the 222 nm CD ellipticity signal after the addition of increasing concentrations of GuCl. Interestingly, at 1.2 M of GuCl, Ni-*Rr*CooJ was still perfectly folded, whereas apo-*Rr*CooJ started to denaturate, as shown by an ellipticity fractional change of 0.09 vs. 0.4, respectively. The midpoint GuCl concentration was determined to be 1.6 M for apo-*Rr*CooJ and 2.0 M for Ni-*Rr*CooJ. This result reveals a higher stability induced by Ni(II)-binding to the protein (Figure 2c).

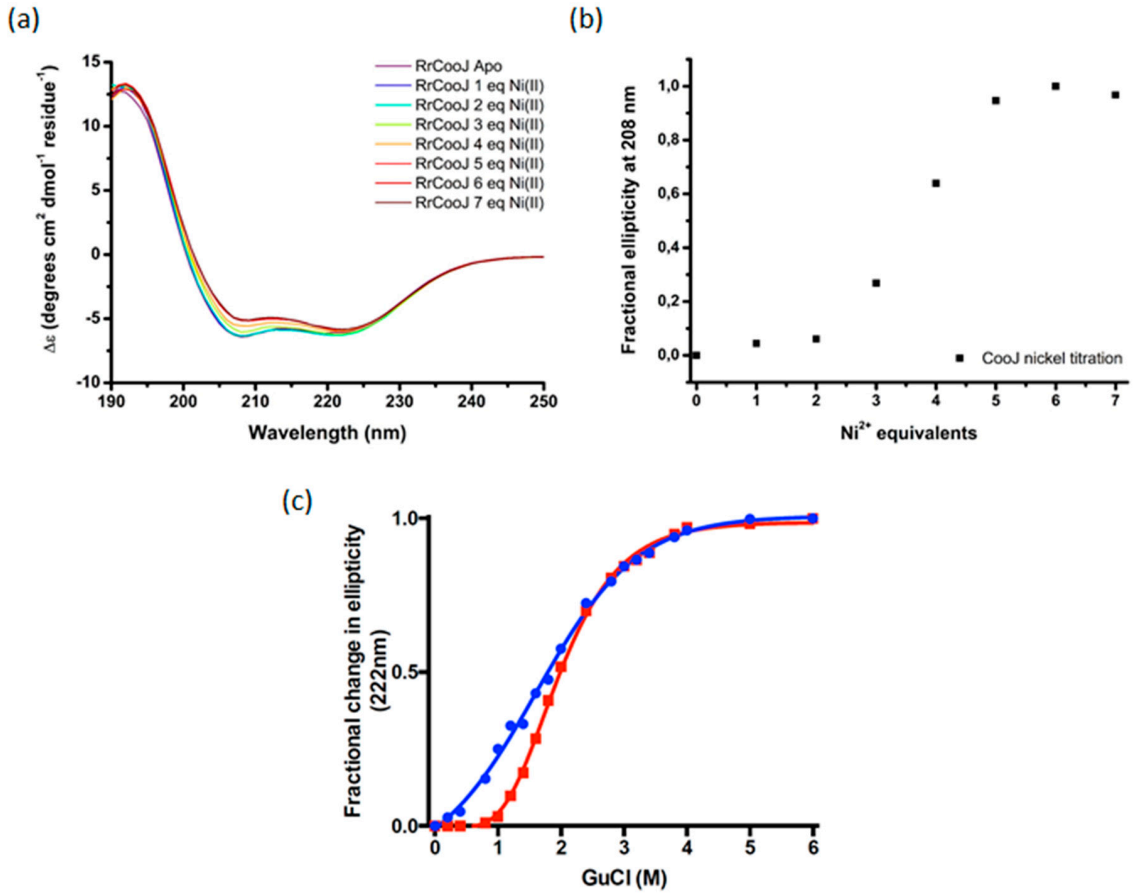

Figure 2. Far-UV circular dichroism (CD) and chemical denaturation of *Rr*CooJ at 4 μM of dimer upon Ni(II) addition. (**a**) Evolution of far-UV signal upon the addition of increasing Ni(II) concentrations. (**b**) Fractional values of the ellipticity registered at 208 nm plotted versus Ni(II) molar equivalents. (**c**) Chemical denaturation of apo-*Rr*CooJ (blue) and Ni-*Rr*CooJ (red) using different concentrations of GuCl at room temperature.

SEC-MALLS experiments were conducted to investigate the oligomeric state of *Rr*CooJ in the presence of Ni(II). We previously showed that a truncated version of *Rr*CooJ (*Rr*CooJ-Δ), lacking the histidine tail (Figure 1), is a stable dimer even in the presence of an excess of nickel [9]. Here, the column was equilibrated with a buffer supplemented with 10 μM of $NiSO_4$, corresponding to a concentration about six times higher than the affinity of the His tails for Ni(II) (Kd = 1.6 μM). The injection of 50 μM of *Rr*CooJ dimer pre-incubated with 5 molar eq. of Ni(II) led to the appearance of a mixture of oligomeric forms ranging from dimers to high-order oligomers (Figure 3a).

To characterize these high-order oligomers, single particle analysis was performed using Transmission Electron Microscopy (TEM). In order to separate the different oligomeric states, size exclusion chromatography was used. Apo-*Rr*CooJ dimer pre-incubated with 5 molar eq. of Ni(II)

was injected onto the column and a series of fractions was selected, based on the SEC-MALLS results. Four samples were collected at different elution volumes (9, 10.5, 13 and 14.5 mL) and subsequently analyzed, revealing the existence of high-order oligomers with sizes ranging from 11 ± 2 nm to 28 ± 5 nm in the three first peaks. In the latter one, corresponding to the elution of *Rr*CooJ tetramers as shown by SEC-MALLS, high-order oligomers could not be detected as expected. Neither aggregation nor fibrils were observed under any of the tested conditions (Figure 3b). The size of high-order oligomers decreased along the elution with an optimum distribution of particles at an elution peak of 13 mL corresponding to a homogenous particle size of about 11 nm.

The oligomerization process is both protein and Ni(II) concentration dependent. Indeed, for a protein concentration of 50 µM of dimer, *Rr*CooJ started to form insoluble aggregates when the Ni(II) concentration reached 500 µM. Moreover, the incubation of 100 µM *Rr*CooJ dimer with 10 molar eq. of $NiSO_4$ (1.0 mM) led to its complete precipitation. However, the addition of 10 mM EDTA can fully redissolve the precipitate within seconds (as shown by protein assay) revealing the easy reversibility of the metal-dependent oligomerization process.

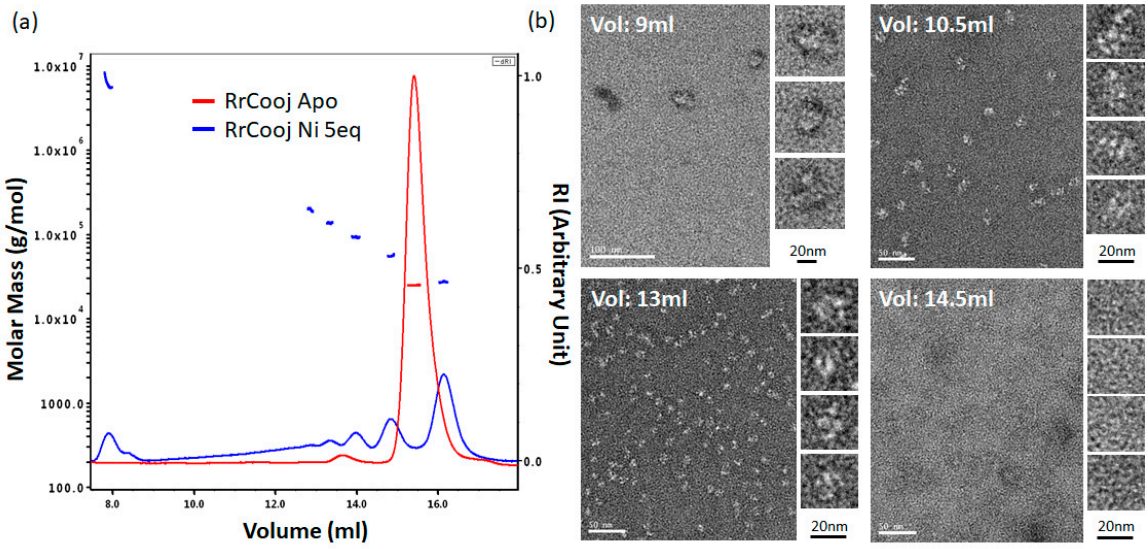

Figure 3. Nickel-dependent oligomerization of *Rr*CooJ by Size Exclusion Chromatography and Multi Angle Laser Light Scattering (SEC-MALLS) and TEM. (**a**) 50 µM of apo-*Rr*CooJ (red) were injected onto a column equilibrated with buffer A (96% of dimer); The injection of 50 µM of *Rr*CooJ dimer preincubated with 250 µM of $NiSO_4$ (blue) in buffer A supplement with 10 µM of $NiSO_4$ shows multiple peaks corresponding to a mixture of oligomers: dimer (35%), tetramer (16%), hexamer (10%), octamer (6.2%) and high-order oligomers (32.8%). (**b**) Nickel-dependent oligomerization analysis of *Rr*CooJ by negative stain after size exclusion chromatography. Image of negatively stained particles (23,000× and 30,000× of magnification) of high-order oligomers of Ni-*Rr*CooJ with highlights of particles measured for the following elution volumes: 9 mL (28 ± 3 nm), 10.5 mL (15 ± 2 nm), 13 mL (11 ± 2 nm) and 14.5 mL (below 5 nm). Oligomer size was determined after merging 20 independents particles by "ImageJ v 1.51" software. Vol: Elution volume.

In order to study their in-cell Ni(II)-binding capability and behavior, *Rr*CooJ and its truncated version *Rr*CooJ-Δ were overproduced in *E. coli* in growth medium supplemented with a range of Ni(II) concentrations from 0 to 2.5 mM $NiSO_4$. As a control, the impact of nickel was evaluated on a strain of *E. coli* transformed with an empty vector. The growth of the control culture was strongly affected by nickel, decreasing remarkably between 0.5 mM and 1.5 mM, and stopping for concentrations higher than 1.5 mM. The presence of *Rr*CooJ or *Rr*CooJ-Δ increases the nickel resistance of *E. coli*, resulting in a constant growth even at high concentration of metal (Figure 4a). Although *Rr*CooJ and *Rr*CooJ-Δ are both able to bind Ni(II) in-cell, we observed that *Rr*CooJ tends to form insoluble oligomers upon addition of increasing concentrations of Ni(II) in the growth medium. At 1.0 mM of $NiSO_4$, despite

a bacterial growth rate similar to the one in the absence of nickel, the overproduced *Rr*CooJ was mainly found in the insoluble fraction, as shown by SDS gel (Figure 4b). This behavior was not observed with the overproduced *Rr*CooJ-Δ, mainly found in the soluble fractions independently on the nickel concentration (Figure 4b). This is a strong indication that the His-tail triggers the oligomerization process of *Rr*CooJ in the presence of nickel, in agreement with the in vitro studies, without drastically affecting the bacterial growth.

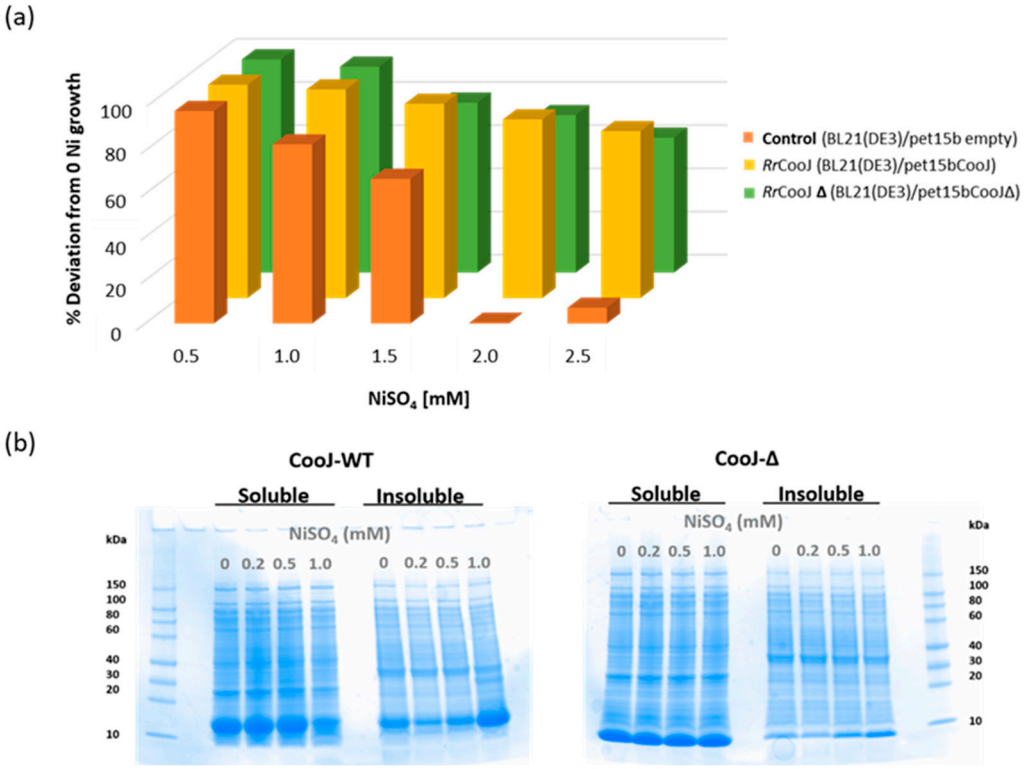

Figure 4. Growth response to nickel content in *E. coli* strains overproducing *Rr*CooJ or *Rr*CooJ-Δ. (**a**) The resistance towards nickel for the control (orange), *Rr*CooJ (yellow) and *Rr*CooJ-Δ (green) cultures is plotted for each different nickel concentration after 16 h from the induction. The resistance is reported as percentile deviation of the OD_{600} measured at 16 h considering as maximum value the OD_{600}-16h measured for the cultures at 0 mM $NiSO_4$ versus the ones measured for the culures at different nickel concentrations. The deviation is calculated using the formula $\sum_{n=1}^{3}\left(\frac{OD_{600\ at\ x\ mM\ 16\ h} - OD_{600\ before\ induction}}{OD_{600\ at\ 16\ h\ for\ O\ mM\ Ni}}\right) * 100$, using the OD_{600}-16h measured for each different nickel concentration ($x\ mM$ = 0.5, 1.0, 1.5, 2.0, 2.5 mM $NiSO_4$). (**b**) SDS-PAGE of soluble and insoluble extracts of *E. coli* cultures overproducing *Rr*CooJ or *Rr*CooJ-Δ in the presence of Ni(II) in the growth media (0 to 1.0 mM $NiSO_4$).

3. Materials and Methods

Recombinant *Rr*CooJ and *Rr*CooJ-Δ were overproduced in *E. Coli* and purified as previously described [9]. Protein concentration was determined either by SEC-MALLS or by Rose Bengal protein assay to determine the protein concentration for the EDTA solubilization experiment.

3.1. Circular Dichroism (CD) Spectroscopy

CD spectra were recorded using a J-1500 circular dichroism spectrometer (JASCO Analytical Instruments, Easton, PA, USA). A stock solution of 10 mM $NiSO_4$ was used to monitor metal-dependent secondary structure content upon Ni(II) titration (from 0 to 7 molar equivalents of $NiSO_4$). Spectra were recorded from 190 to 250 nm using a 1 mm cuvette, with ten accumulations to increase the signal-to-noise ratio. Proteins were thawed and diluted to 4 µM dimer in CD buffer (5 mM potassium phosphate pH

7.0, containing 0.5 mM TCEP). For the determination of the secondary structure elements, the spectra were analyzed using the BeStSel online software [12]. The guanidine hydrochloride denaturation experiments were performed via additions of different concentrations of GuCl on 4 μM dimer samples (apo- and Ni-*Rr*CooJ), followed by 2 h of incubation. The Ni-*Rr*CooJ sample was prepared by adding 5 molar equivalents of Ni(II) per protein dimer (20 μM final concentration) and incubated for 30 min prior to its denaturation. The fractional change in ellipticity at 222 nm was used to determine the variation of the secondary structure elements due to the denaturation of the protein. Empiric fit was done via a sigmoidal equation.

3.2. Size Exclusion Chromatography and Multi Angle Laser Light Scattering (SEC-MALLS)

Purified and frozen *Rr*CooJ was thawed and diluted to 50 μM of dimer in 50 mM HEPES pH 7.5, 150 mM NaCl, 1 mM TCEP (buffer A). Ni-*Rr*CooJ was incubated in the presence of 250 μM $NiSO_4$ for 30 min at room temperature prior to injection onto the SEC-MALLS system (Wyatt Dawn HELEOS-II 18-angle light scattering detector and Wyatt Optilab rEX refractive index monitor linked to a Shimadzu HPLC system comprising a LC-20AD pump, a SPD20A UV/Vis detector, and a Superdex 200 10/300 increase column (GE Healthcare Life Sciences, Pittsburg, KS, USA). Injections were carried out using a 20 μL loop. The size exclusion column was equilibrated using buffer A ± 10 μM $NiSO_4$. Protein concentration in all samples was determined by integration of the differential refractive index (dRI) peak (dn/dc = 0.185). It is important to note that all used samples came from the same stock protein. The data were analyzed using the ASTRA software (version 6) (WYATT Technology Corporation, Santa Barbara, CA, USA).

3.3. Electron Microscopy

100 μL of Ni-*Rr*CooJ dimer at 50 μM were injected onto a Superdex 200 10/300 column (GE Healthcare) equilibrated with buffer A + 10 μM $NiSO_4$. 200 μL-fractions were collected and 4 fractions corresponding to elution volumes of 9, 10.5, 13 and 14.5 mL were selected. The negative stain Mica-carbon Flotation Technique (MFT) was used to prepare the samples. Briefly, 3–5 μL of protein sample (0.1 to 0.01 mg/mL) were applied to a clean side of a carbon layer (between a carbon and a mica layer). The carbon was then floated on stain (2% *w/v* uranyl acetate (AcU) pH 4.5) and covered by a copper grid. The images were captured under low-dose conditions (<10 e− $Å^{-2}$) at a magnification of 23K× and 30K× with defocus values between 1.2 and 2.5 μm on a Tecnai 12 LaB6 electron microscope at 120 kV accelerating voltage using a CCD Camera Gatan Orius 1000 (Gatan, Inc., Pleasanton, CA, USA).

3.4. Growth Response to Nickel in E. coli Strains Overproducing RrCooJ or RrCooJ-Δ

E. coli BL21 (DE3) strain was transformed with pET15b, pET15b-*Rr*CooJ or pET15b-*Rr*CooJ-Δ. The three different cultures (100 mL each) were grown in LB medium, with the appropriate antibiotic, at 25 °C and 180 rpm to an OD_{600} of ~0.6 and induced with 0.25 mM IPTG. At this point, each culture was divided into five 50 mL-Falcon tubes (10 mL-culture each) and a range of $NiSO_4$ concentrations was added to the culture medium (0, 0.5, 1.0, 1.5, 2.0 and 2.5 mM). The cells were grown overnight at 25 °C and 180 rpm, and the OD_{600} was measured after 16 h for all the cultures. The cultures were done in triplicate for each different condition. The effect of the overproduction of *Rr*CooJ or *Rr*CooJ-Δ according to the amount of Ni(II) was evaluated by normalizing the culture optical densities, measured at the different nickel concentrations, with the values obtained from the control. To study the solubility of *Rr*CooJ in the presence of Ni(II) in-cell, *E. coli* BL21 (DE3) strain transformed with either pET15b-*Rr*CooJ or pET15b-*Rr*CooJ-Δ were grown as described above, except that 25 mL-cultures were grown in 50 mL-flasks with 0, 0.2, 0.5 and 1.0 mM $NiSO_4$ concentration. After overnight growth, the OD_{600} was measured (5.5 ± 0.2 for BL21(DE3)/pET15b-*Rr*CooJ-Δ cultures and 5.8 ± 0.3 for BL21(DE3)/pET15b-*Rr*CooJ cultures). The cell pellets were collected by centrifugation and then resuspended in 4 mL of 50 mM Tris-HCl, pH 8.0 containing a complete Protease Inhibitor cocktail tablet (Roche Life Science, Indianapolis, IN, USA). After three freeze-thaw cycles, the cultures were sonicated

and centrifuged at 14,000 rpm for 20 min. The 16 pellets were resuspended in 50 mM Tris-HCl pH 8.0, containing 4 M urea and 0.1% SDS. Ten microliters of each sample were examined using SDS-PAGE (Bio-Rad Corporate, Hercules, CA, USA).

4. Conclusions

Recently, structural studies of apo-*Rr*CooJ revealed its atypical topology with two independent histidine tails flanking a central coiled coil region. Here, we focused our attention on the histidine-rich region behavior. Two phenomena were observed upon nickel addition. Firstly, Ni(II)-binding directly impacts the secondary structure content of the protein, with a gain in α-helices related to higher stability. Secondly, nickel induces a dynamic and reversible oligomerization process in vitro, leading to the protein precipitation observed both in vitro and in cellulo, in the presence of elevated Ni(II) levels. Further studies are necessary to investigate the functional role of *Rr*CooJ oligomerisation in nickel homeostasis under physiological conditions.

Author Contributions: Conceptualization, C.C. and M.A.; formal analysis, C.C., M.A., J.P.; investigation, C.C., M.A.; writing—original draft preparation, C.C.; writing—review and editing, M.A.

Funding: This work was supported by "the ITERLIS PhD program, CEA Life sciences" for MA's PhD funding, the "FUNBIOCO" project (IDEX-UGA, Initiatives de Recherche stratégiques) and the "COSYNBIO" project (Projets exploratoires, Cellule energie-CNRS). This work has been partially supported by Labex ARCANE and CBH-EUR-GS (ANR-17-EURE-0003). The research leading to these results has received funding from the networking support from the COST Action FeSBioNet (Contract CA15133).

Acknowledgments: This work used the platforms of the Grenoble Instruct Centre (ISBG; UMS 3518 CNRS-CEA-UJF-EMBL) with support from FRISBI (ANR-10-INSB-05-02) and GRAL (ANR-10-LABX-49-01) within the Grenoble Partnership for Structural Biology (PSB). The electron microscope facility is supported by the Rhône-Alpes Region, the Fondation Recherche Medicale (FRM), the fonds FEDER, the Centre National de la Recherche Scientifique (CNRS), the CEA, the University of Grenoble, EMBL, and the GIS-Infrastrutures en Biologie Santé et Agronomie (IBISA). We thank Daphna FENNEL and Dr Guy SCHOEHN, from the Electron Microscopy platform of the Integrated Structural Biology of Grenoble (ISBG, UMI3265).

Conflicts of Interest: The authors declare no conflicts of interest.

References

1. Kung, Y.; Drennan, C.L. A role for nickel–iron cofactors in biological carbon monoxide and carbon dioxide utilization. *Curr. Opin. Chem. Biol.* **2011**, *15*, 276–283. [CrossRef] [PubMed]
2. Dobbek, H.; Svetlitchnyi, V.; Gremer, L.; Huber, R.; Meyer, O. Crystal structure of a carbon monoxide dehydrogenase reveals a [Ni–4Fe–5S] cluster. *Science* **2001**, *293*, 1281–1285. [CrossRef] [PubMed]
3. Drennan, C.L.; Heo, J.; Sintchak, M.D.; Schreiter, E.; Ludden, P.W. Life on carbon monoxide: X-ray structure of Rhodospirillum rubrum Ni–Fe–S carbon monoxide dehydrogenase. *Proc. Natl. Acad. Sci. USA* **2001**, *98*, 11973–11978. [CrossRef] [PubMed]
4. Alfano, M.; Cavazza, C. The biologically mediated water–gas shift reaction: Structure, function and biosynthesis of monofunctional [NiFe]-carbon monoxide dehydrogenases. *Sustain. Energy Fuels* **2018**, *2*, 1653–1670. [CrossRef]
5. Kerby, R.L.; Ludden, P.W. In vivo nickel insertion into the carbon monoxide dehydrogenase of Rhodospirillum rubrum: Molecular and physiological characterization of cooCTJ. *J. Bacteriol.* **1997**, *179*, 2259–2266. [CrossRef] [PubMed]
6. Singer, S.W.; Hirst, M.B.; Ludden, P.W. CO-dependent H2 evolution by Rhodospirillum rubrum: Role of CODH: CooF complex. *Biochim. Biophys. Acta Bioenerg.* **2006**, *1757*, 1582–1591. [CrossRef] [PubMed]
7. Jeon, W.B.; Cheng, J.; Ludden, P.W. Purification and Characterization of Membrane-associated CooC Protein and Its Functional Role in the Insertion of Nickel into Carbon Monoxide Dehydrogenase from Rhodospirillum rubrum. *J. Biol. Chem.* **2001**, *276*, 38602–38609. [CrossRef] [PubMed]
8. Watt, R.K.; Ludden, P.W. The Identification, Purification, and Characterization of CooJ. *J. Biol. Chem.* **1998**, *273*, 10019–10025. [CrossRef] [PubMed]

9. Alfano, M.; Pérard, J.; Carpentier, P.; Basset, C.; Zambelli, B.; Timm, J.; Crouzy, S.; Ciurli, S.; Cavazza, C. The carbon monoxide dehydrogenase accessory protein CooJ is a histidine-rich multidomain dimer containing an unexpected Ni(II)-binding site. *J. Biol. Chem.* **2019**, *294*, 7601–7614. [CrossRef] [PubMed]
10. Iadanza, M.G.; Jackson, M.P.; Hewitt, E.W.; Ranson, N.A.; Radford, S.E. A new era for understanding amyloid structures and disease. *Nat. Rev. Mol. Cell Biol.* **2018**, *19*, 755–773. [CrossRef] [PubMed]
11. Ge, R.; Zhang, Y.; Sun, X.; Watt, R.M.; He, Q.-Y.; Huang, J.-D.; Wilcox, D.E.; Sun, H. Thermodynamic and Kinetic Aspects of Metal Binding to the Histidine-rich Protein, Hpn. *J. Am. Chem. Soc.* **2006**, *128*, 11330–11331. [CrossRef] [PubMed]
12. Micsonai, A.; Wien, F.; Bulyáki, É.; Kun, J.; Moussong, É.; Lee, Y.-H.; Goto, Y.; Réfrégiers, M.; Kardos, J. BeStSel: A web server for accurate protein secondary structure prediction and fold recognition from the circular dichroism spectra. *Nucleic Acids Res.* **2018**, *46*, W315–W322. [CrossRef] [PubMed]
13. Kwok, S.C.; Hodges, R.S. Stabilizing and destabilizing clusters in the hydrophobic core of long two-stranded α-helical coiled-coils. *J. Biol. Chem.* **2004**, *279*, 21576–21588. [CrossRef] [PubMed]